

# Demonstration of entanglement distribution over 155 km metropolitan fiber using a silicon nanophotonic chip

Jinyi Du<sup>1\*</sup>, Xingjian Zhang<sup>1\*</sup>, George F.R. Chen<sup>2</sup>, Hongwei Gao<sup>2</sup>,  
Dawn T. H. Tan<sup>2,3\*</sup>, Alexander Ling<sup>1,4\*</sup>

<sup>1</sup>\*Centre for Quantum Technologies, National University of Singapore, 3  
Science Drive 2, Singapore, 117543, Singapore.

<sup>2</sup>Photonics Devices and System Group, Singapore University of  
Technology and Design, 8 Somapah Rd, Singapore, 487372, Singapore.

<sup>3</sup>Institute of Microelectronics, Agency for Science Technology and  
Research (A\*STAR), 2 Fusionopolis Way, #08-02 Innovis Tower,  
Singapore, 138634, Singapore.

<sup>4</sup>Department of Physics, National University of Singapore, 2 Science  
Drive 3, Singapore, 117551, Singapore.

\*Corresponding author(s). E-mail(s): [jinyidu@u.nus.edu](mailto:jinyidu@u.nus.edu);  
[xingjianzhang@u.nus.edu](mailto:xingjianzhang@u.nus.edu); [dawn.tan@sutd.edu.sg](mailto:dawn.tan@sutd.edu.sg);  
[alexander.ling@nus.edu.sg](mailto:alexander.ling@nus.edu.sg);

## Abstract

Transmitting an entangled state over an extended distance is crucial for the development of quantum networks. Previous demonstrations of transmitting entangled photons over long distance using satellites or fibers have used entangled photon pairs generated from bulk crystal arrangements. An alternative approach would be to generate photon pairs using silicon-on-insulator (SOI) chips. Despite numerous proof-of-concept studies, no long range distribution has been achieved using this platform because of the challenge of getting sufficient off-chip brightness. We report a SOI platform that provides an off-chip entangled photon pair brightness of between 8,000 to 460,000 pairs per second. This exceeds previous reports by three orders of magnitude in brightness. The entanglement fidelity is 99.85(6)% and 97.90(3)% respectively. Measuring one photon locally, and transmitting the other over 93 km of deployed fiber (link loss of 40 dB), achieves a count rate of 132 pairs per second with an entanglement fidelity of 93.3(3)%, after solving the

additional challenges of chromatic dispersion. The source can be pumped harder to enable transmission of entangled photons over 155 km of deployed fiber (link loss of 66 dB) at a rate of 0.7 pairs per second, with an entanglement fidelity of 87.6(5)%. These results demonstrate that SOI nanophotonic chips can perform competitively with bulk crystal sources and represent an important step toward building quantum networks using integrated nanophotonic platforms.

**Keywords:** Entanglement distribution, Silicon nanophotonic chip, Quantum entanglement

## 1 Introduction

Entanglement distribution will be important for building quantum networks that provide secure communications or novel services such as blind quantum computing. Impressive distances have been achieved using satellite-based entanglement technology [1–4], or with terrestrial free-space links using telescopes [5, 6]. For dense urban environments, however, optical fibers provide an alternative channel that is not limited by atmospheric conditions. Fiber-based polarization entanglement has been successfully distributed over distances up to 248 km [7–9].

A common feature of the experiments above is that the entangled photon pairs have been generated using nonlinear crystals such as bulk PPLN [7–9] or PPKTP [10]. AlGaAs chip-based sources have been explored for a 50 km fiber spool [11]. Long distance polarization entanglement distribution using photon pairs obtained from CMOS-compatible silicon nanophotonic chips have not yet been demonstrated. To overcome the link loss over long fiber stretches, the photon pair sources need to be very bright and to-date silicon photonic chips have not provided high off-chip brightness due to coupling losses [12–15]. In contrast, bulk optical systems are several orders of magnitude brighter than their chip-based counterparts.

We report a bright entangled photon pair source based on a silicon nanophotonic chip that can distribute entanglement through approximately 66 dB of loss, corresponds to 155 km of deployed optical fiber in a metropolitan network. By using a novel edge coupler [16], the silicon chip is placed in a Sagnac configuration and enables direct observation of entangled photon pairs at a rate of 460,000 pairs/second. This off-chip brightness is three orders of magnitude higher than previous reports [17, 18], enabling long-distance entanglement distribution.

The entangled photons experience significant chromatic dispersion over the long distance deployed fiber route. This is compensated by using a nonlocal dispersion compensation technique [9, 19, 20] that results in an improvement in the coincidence-to-accidentals ratio (CAR) and two-photon interference theoretical fidelity by 32%. This result demonstrates that the CMOS chip sources have competitive performance when compared to sources using bulk nonlinear optics.

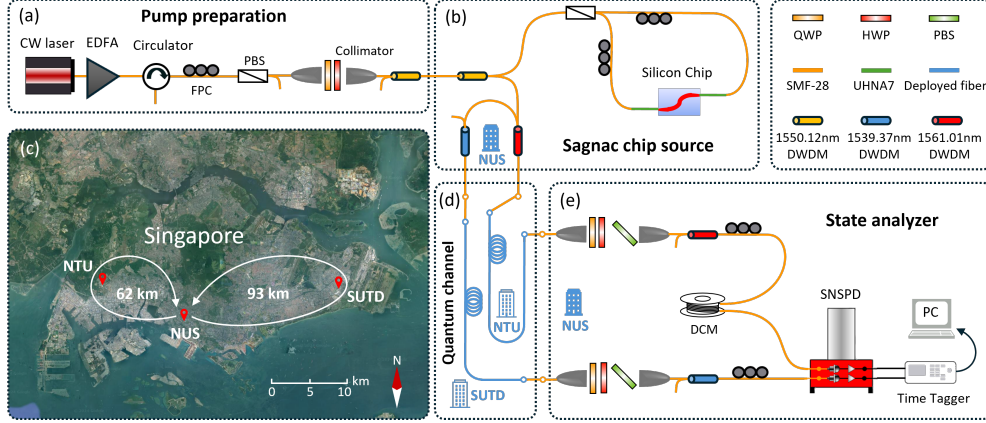


**Fig. 1 Entanglement distribution over 155 km deployed fiber.** (a, b) A continuous-wave laser at 1550.12 nm facilitates the generation of photon pairs in a polarization-entangled state through spontaneous four-wave mixing (SFWM), enabled by the sagnac configuration. The nondegenerate photon pairs are wavelength-separated using a dense wavelength-division multiplexer (DWDM). (c) One fiber runs from the National University of Singapore (NUS) to the Singapore University of Technology and Design (SUTD) and back to NUS via a second fiber follows a circuitous path, resulting in a total length that exceeds the straight-line distance between these locations. Another fiber runs from NUS to Nanyang Technological University (NTU) and back to NUS via a second fiber. (d) The signal photon (1539.37 nm) travels through the SUTD route while the idler photon (1561.01 nm) travels through the NTU route. The deployed fibers can be replaced with patchcord fiber when measuring the source entanglement fidelity. (e) The photons are eventually detected by a superconducting nanowire single-photon detector (SNSPD) at NUS. To correct for fiber birefringence, fiber polarization controllers (FPC) and quarter-wave plates (QWP) are utilized. Half-wave plates (HWP) facilitate the switching between horizontal (H), vertical (V), diagonal (D), and anti-diagonal (A) polarizations. Polarization beam splitters (PBS) in the setup are used to either purify the polarization states or evenly split the H and V components within the Sagnac loop. A dispersion compensation module (DCM) is placed on the idler photon arm before the SNSPD to provide nonlocal dispersion compensation.

## 2 Results

### 2.1 On-chip entangled photon generation

The experimental setup for generating polarization entangled photons is illustrated in Fig. 1.(a, b). The test utilizes a nanophotonic chip that is an 8 mm long silicon waveguide, equipped with edge couplers at both ends, each exhibiting a loss of 0.64 dB. The silicon chip is integrated into a Sagnac fiber loop consisting of a PBS and two FPC on each arm. A continuous-wave (CW) laser with a wavelength of 1550.12 nm first passes through a standard dense wavelength division multiplexer (DWDM) filter and is then evenly split by the PBS. The vertically polarized (V) beam is converted to horizontal polarization (H) with fiber polarization controllers (FPC) before entering the chip. A short section of 2.4  $\mu\text{m}$  small-core fiber (UHNA7), less than 1 cm in length, is spliced to the tip of coupling fiber to assist mode conversion with a splicing loss of 0.03 dB.

A pump beam injected into the chip causes spontaneous four wave mixing (SFWM) to occur. A pair of pump photons at frequency  $\omega_{pump}$  are annihilated, generating a new photon pair, following the energy conservation equation  $2\omega_{pump} = \omega_{signal} + \omega_{idler}$ . [21] To create entangled photon pairs, the pump is injected from both ends of the waveguide simultaneously, leading to the generation of photon pairs propagating in both directions. These pairs can be collected from either side of the waveguide using the same fiber as pump laser. One pair is horizontally (H) polarized and the other pair is converted to vertically (V) polarized by FPC. As the H and V state photons travel through the same fiber, no phase shift occurs between the two arms. By superposing the H and V polarized photon pairs from both paths at the PBS, the maximally entangled Bell state is constructed at the output port of the PBS:

$$|\Phi\rangle = \frac{1}{\sqrt{2}}(|HH\rangle + |VV\rangle), \quad (1)$$

The entangled photons are reflected by a DWDM module centered at 1550.12 nm to the reflection arm. A narrow band portion (0.8 nm) of photon pairs are then separated using 100 GHz DWDM modules centered at 1561.01 nm (idler) and 1539.37 nm (signal). The broadband nature of the entangled photons generated from the SFWM process in the straight Si waveguide allows for the cascading of additional filters to multiplex more channels of entangled photons. [11, 14]

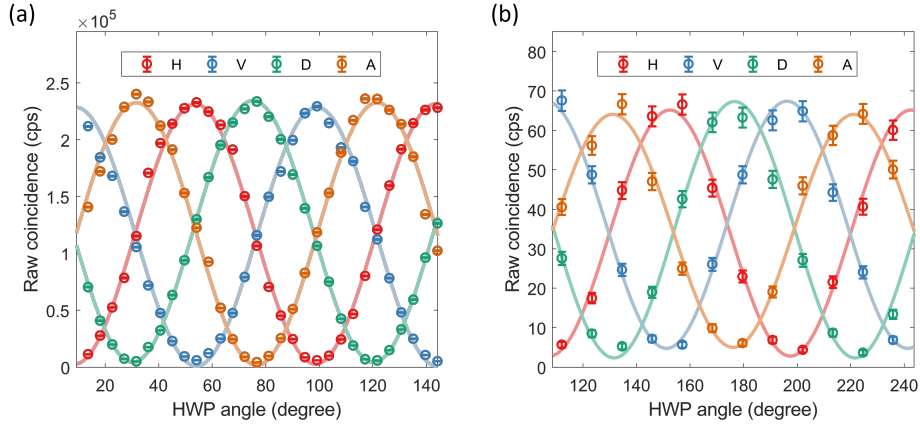


**Fig. 2 Two fold coincidence curves.** (a) Coincidence measurement of entangled source. The signal photon's HWP angle  $\theta_s$  is fixed at H, V, D, and A basis, while the idler photon's HWP angle  $\theta_i$  rotates for  $180^\circ$ . (b) Entanglement characterization with signal photons travel through 93 km of deployed fiber. Accidental counts 1.6 cps are not subtracted.

## 2.2 Entangled source characterization

Once the signal and idler photons are filtered, they first pass through two quarter-wave plates (QWP) to compensate for polarization distortion caused by the connecting

fibers. Each arm of the entangled photons are then projected into different polarization bases, using half-wave plates (HWP) and polarizing beam splitters. During source characterization, a short length of fiber replaces the deployed fibers, directly connecting the source to the measurement setup.

The HWP in the signal arm is fixed at  $\theta_s$ , while the HWP in the idler arm rotates for  $180^\circ$ . Photons are detected by SNSPDs, with the coincidence count recorded during the rotation. The single photons are detected with SNSPDs, with the efficiency for idler channel at 45% while efficiency for signal channel is at 49%. Fig. 2.(a) displays the observed raw coincidence rate as a function of  $\theta_i$ .

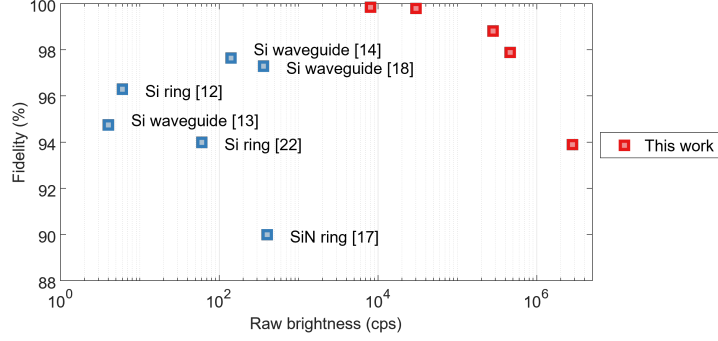


**Fig. 3 Entangled source performance comparison.** The source brightness and fidelity at different pump power are measured and compared the experimental data with other CMOS chip studies.

**Table 1** Comparison with CMOS polarization entangled sources

Source type	Detector (eff.)	Brightness (cps)	Fidelity	Ref
Si waveguide	APD (10%)	4	94.8(41)%	[13]
Si waveguide	APD (20%)	140	97.7(8)%	[14]
Si waveguide	SNSPD (85%)	360	97.3(16)%	[18]
Si ring	SPD (10%)	6	96.3(15)%	[12]
Si ring	SNSPD (81%)	60	94(2)%	[22]
SiN ring	SNSPD (60%)	400	90.0(-)%	[17]
Si waveguide	SNSPD (45%, 49%)	8,000	99.85(6)%	This work
	SNSPD (45%, 49%)	30,000	99.80(4)%	
	SNSPD (45%, 49%)	280,000	98.82(3)%	
	SNSPD (45%, 49%)	460,000	97.90(3)%	
	SNSPD (56%)	2,800,000*	93.9(7)%	

\*This is measured with a 15 dB attenuator inserted in both the signal and idler arms before the SNSPDs to avoid detector saturation. The decreasing fidelity with increasing brightness is due to the number of multiple photon pairs present within the coincidence time window of this system. This effect can be further minimized if the system timing jitter and coincidence window is reduced.

The maximum observed coincidence at the peak of the coincidence curves is 230 kcps, corresponding to an overall brightness of 460,000 entangled photon pairs a

second. The fidelity to the bell state is 97.90(3)%. This source is over 3 orders of magnitude brighter than sources in other literature reports. This comparison is provided in Fig. 3. When the source is operating at low brightness conditions, fidelity can be enhanced to 99.85(6)%, and the experimental data detailed in Table 1.

### 2.3 Asymmetric entanglement distribution over 93 km distance

The signal photons are first connected to the NUS-SUTD-NUS deployed fiber which is 93 km, exhibiting a 35.4 dB loss as measured by an optical time domain reflectometer (OTDR). The idler photons are detected at the source. The propagation loss is calculated to be 0.38 dB/km, which is higher than the typical 0.16 dB/km observed in fiber spools or 0.25 dB/km in submarine fibers [7, 8]. This increased loss is primarily due to the connection junctions in practical metropolitan fibers. When the dispersion compensation module (DCM) is added, 4.3 dB extra loss is also included to the fiber system.

To evaluate the entanglement quality after transmission through the NUS-SUTD-NUS fiber loop, we perform two-fold coincidence measurements equivalent to local testing. The idler arm’s polarization analysis setup is set to H, V, D, and A bases. The signal arm’s HWP is rotated through 180° to measure the visibility. As shown in Fig. 2.(b), observed raw count rate of entangled photons is 132 cps, while the fidelity is 93.3(3)% in the 10 second measurement duration. The high fidelity attributed to effective background count filtering and nonlocal dispersion compensation.

**Table 2** Comparison with other long fiber works

Source type	Fiber type	Fiber loss	DOF	Rate (cps)	Fidelity	Ref
Sagnac PPLN	Submarine (96 km)	22 dB	pol.	366	95.3(3)%	[7]
Sagnac PPLN	Submarine (192 km)	48 dB	pol.	8.6	95(1)%	[8]
Sagnac PPLN	Metropolitan (248 km)	71.5 dB	pol.	9	93(-)%	[9]
Sagnac PPLN	Ultra low loss spool (404 km)	87 dB	pol.	0.03	91.3(-)%	[23]
Sagnac	Metropolitan (93 km)	39.7 dB	pol.	132	93.3(3)%	This work
Si chip	Metropolitan (155 km)	66 dB		0.7	87.6(5)%	

### 2.4 Symmetric entanglement distribution over 155 km deployed fiber

When only the signal photons are deployed, the timing delay between the signal and idler arms are observed to experience a cyclic drift. This cyclic drift is attributed to diurnal temperature fluctuations that cause the length of the fibers to expand and contract. This effect is reduced when both signal and idler photons are deployed over

similar lengths of fiber. This “symmetric” experiment was performed by connecting the idler photons to a fiber loop that connected NUS and NTU. In this setup, the overall length traversed by the photon pair exceeds 155 km, and the overall system loss reached 66 dB (56 dB from fiber, 10 dB from DCM). By increasing the pump power, the entangled photon pair rate after transmission was 0.7 cps with a fidelity of 87.6(5)%. Accounting for fiber loss, the off-chip photon pair rate was 2.8 Mcps and the estimated fidelity was 93.9(7)% as shown in Fig. 3. The degradation is primarily due to the effects of polarization mode dispersion (PMD). [9, 24–27] A comparison of the results from this work with similar work in the literature regarding fiber-based entanglement distribution is provided in Table 2.

### 3 Conclusion

In this report we have demonstrated a bright entangled photon pair source based on a silicon nanophotonic chip. The source was sufficiently bright that entanglement could be distributed over 66 dB of loss (in our experiment this is equivalent to 155 km of deployed fiber and a dispersion compensation module). The observed brightness and fidelity of the nanophotonic chip source is competitive when compared against work based on bulk crystal sources. [7–9] This work marks a milestone in the capability of silicon nanophotonic chips for enabling long range quantum networks. This source is also useful for satellite to ground experiments because it exceeds the loss of the Micius double-downlink where the link loss was 62 dB. [2, 28].

There are a number of avenues for further integration and improvement. For example, many of the filters are based on fiber components and further integration [29–31] is possible in this aspect enhancing the stability and scalability of the setup. We note also that the nonlocal dispersion compensation is performed using a dispersion compensated module that has a significant transmission loss, which should be reduced with further engineering [32, 33]. We note also that there is a huge potential for utilising dense-wavelength division multiplexing with the silicon nanophotonic chip. This will expand the number of channels accessible. [22, 23, 34] Finally, other degrees of freedom, such as the time-bins could be added to the setup. [35–37] Taken together, these modifications will dramatically increase the capacity for quantum information transfer within the network.

## 4 Methods

### 4.1 Chip design and coupling strategy

The chip involved in the experiment is a 8 mm long silicon waveguide with cross sectional dimension 650 nm in width and 250 nm in height. The whole chip is covered by 2  $\mu$ m thick SiO<sub>2</sub> cladding layer. On the chip edges, two-stage inverse tapers are fabricated to expand the chip mode to reduce the mode mismatch with that of the UHNA7 fiber. The L0 section acts as buffer region to protect the edge coupler during dicing process, while the length of L1 and L2 tapers are 50  $\mu$ m and 100  $\mu$ m respectively. Short section of UHNA7 fiber (less than 1 cm) is spliced to SMF-28 fiber to assist light collection. The loss is optimized to 0.03 dB per splicing junction by performing

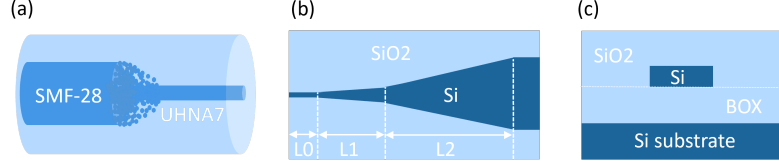


**Fig. 4** (a) Fiber splicing junction showing the tapered region that adiabatically converts the UHNA7 fiber mode to SMF-28. (b) Top view of the two-stage inverse taper edge coupler with a BOX layer; upper cladding not shown. (c) Cross-sectional view of a silicon chip with a silicon waveguide above a  $2\ \mu\text{m}$  BOX layer, covered by  $2\ \mu\text{m}$  SiO<sub>2</sub> cladding.

an in-situ monitoring of the loss during splicing process. [16] The measured coupling loss is 0.64 dB per facet and has nice long term stability of  $\pm 0.02$  dB for more than ten days without using any adhesive.

## 4.2 Photon pair wavelength selection

In the SFWM process, two pump photons are absorbed simultaneously, elevating the system to a virtual energy level, followed by the emission of a signal and idler photon to conserve both energy and momentum. The efficiency of this nonlinear interaction is highly dependent on the phase matching conditions. The coincidence-to-accidentals ratio (CAR) quantifies the ratio of true photon coincidences (from genuine photon pairs) to accidental coincidences, such as those arising from multi-photon emissions or system noise. A high CAR is essential for ensuring high entanglement fidelity, as it directly correlates with the purity of the detected entangled state by reducing the likelihood of accidental events degrading the measurement. Therefore, maximizing CAR requires lower multi-photon events and system noise, such as residual pump photons and Raman noise.

To select the optimal wavelengths for the highest CAR and entangled photon quality, a 1550.12 nm CW laser is employed to unidirectional pumping for the same chip used in the entanglement generation experiment. The generated photon pairs, signal and idler, were spectrally broad due to the nature of phase matching in silicon. Two 0.8 nm bandwidth filters with central wavelength symmetrical about the pump are installed to scan the pair generation rate across different wavelength channels.

As illustrated in Fig. 5.(a), the raw photon coincidence rate was highest when the signal and idler wavelengths were closest to the pump wavelength, indicating that phase matching was most efficient at shorter detunings from the pump. However, this increased photon pair generation does not directly translate into a higher CAR, as shown in Fig. 5.(b), where the CAR peaks approximately 10 nm away from the pump wavelength. This discrepancy can be explained by the balance between photon pair generation and system noise. While photon pairs are generated more efficiently near the pump wavelength, the proximity of the signal and idler to the pump results in less effective rejection of residual pump photons as shown in Fig. 5.(c). These residual pump photons contribute to accidental coincidences, lowering the CAR. On the other hand, when the signal and idler photons are too far from the pump, the SFWM process itself becomes less efficient, reducing the photon pair generation rate and thereby



lowering the CAR due to the lower coincidence rate. The observed peak in CAR at a 10 nm separation from the pump wavelength results from the optimal trade-off between reducing system noise and maintaining sufficient photon pair generation.

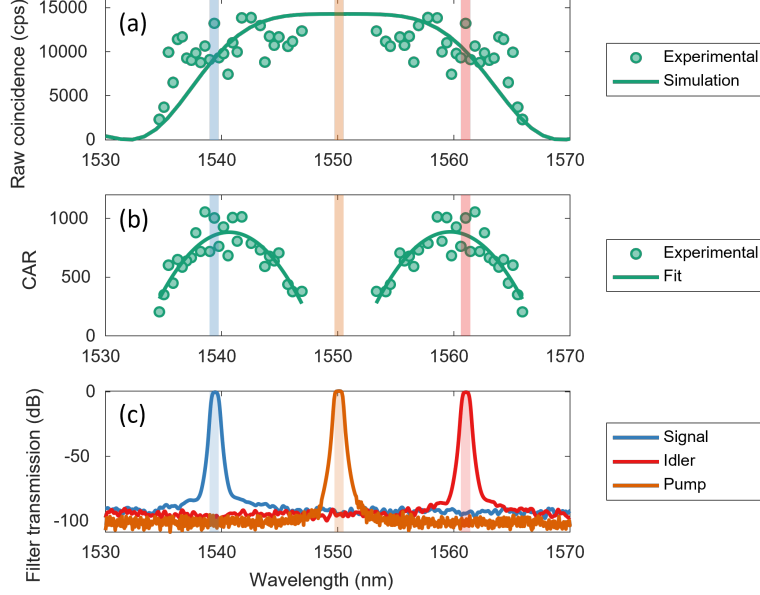


**Fig. 5 Observed photon pair rate, CAR, and filter transmission as functions of wavelength.** (a) Raw coincidence rate as a function of signal and idler wavelengths relative to the pump, showing that photon pair generation is most efficient near the pump wavelength due to optimal phase matching. (b) Coincidence-to-accidental ratio (CAR) as a function of wavelength. The CAR peaks approximately 10 nm away from the pump, where pump photon rejection is optimal. (c) Transmission profiles of the filters used for signal, idler, and pump photons, with an extinction ratio of approximately 80-100 dB, indicating the optimal filter performance at a 5-10 nm separation from the center wavelength.

### 4.3 Methods to improve the fidelity

In this experiment the deployed fiber is not dark and contains broadband noise within the optical channel of interest. This noise lowers the CAR value affecting the fidelity of the observed quantum state. The relationship between fidelity and CAR is given by  $F = \frac{CAR}{CAR+1}$ . A 0.8 nm filter is installed before the SNSPDs, and the dark count noises are effectively removed from around 4 Mcps to less than 200 cps. The CAR is increased from 2 to 15, which corresponds to a theoretical fidelity improvement from 67% to 94%.

Additionally, chromatic dispersion presents a significant challenge to achieving high entanglement fidelity. The dispersion value at 1539 nm is around  $D_{1539} \leq 18.0$  ps/(nm·km) in the fiber. Since the bandwidth of signal photons is 0.8 nm while the

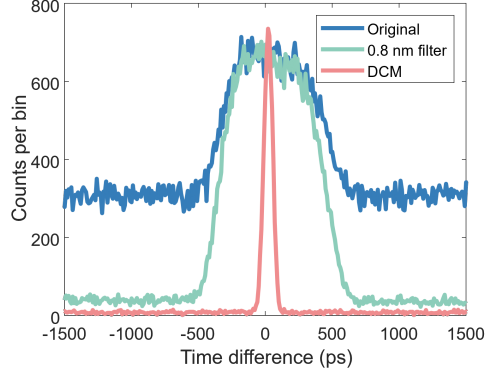


**Fig. 6 Coincidence count measured per bin.** The peaks are in the center of the cross-correlation function between the time tag files obtained from the two SNSPD channels. The time delay  $457 \mu\text{s}$  between the two channels is already compensated digitally. The blue line is the original histogram shape after the long fiber transmission. The green line is the histogram with dark count noise filtering. After nonlocal dispersion compensation, the FWHM of the histogram peak is greatly reduced and plotted in red line.

fiber distance is 93 km, the dispersion caused by the deployed fiber is 1339 ps. In comparison, the overall timing jitter of the SNSPDs including the time tagger, is approximately 80 ps. As a result, measuring the photon pair rate after signal photons transmitted through the long fiber requires a larger coincidence window around 1 ns. This larger coincidence window increases accidental counts, greatly reducing the CAR value. To solve this, a dispersion compensation module (DCM) is inserted in the idler arm. The total dispersion compensation provided by the DCM at 1561 nm is around -1360 ps/nm, as data provided by the manufacturer. Effective dispersion compensation raises the CAR from 15 to 91, corresponding to an increase in theoretical fidelity from 94% to 99%. However, the measured fidelity in practice is lower than this theoretical value, primarily due to the effects of PMD. It is important to note that the DCM introduces 4.3 dB insertion loss, which does impact the coincidence rate. This DCM-related loss may be mitigated in future work where the waveguide platform could be designed to generate photons with narrower wavelength bandwidth. [12, 17, 22, 38, 39]

#### 4.4 System calibration

The polarization shift caused by birefringence is compensated by the QWP and HWP in the measurement setup. To calibrate the system once the NUS-NTU-NUS quantum channel is established, we disconnect the H polarization arm of Sagnac loop and inject a 13 dBm laser beam at 1561.01 nm into the setup. This wavelength matches that of the idler photons, allowing the laser to go through the same route as idler photons do. After transmission through the PBS in the measurement setup, the laser is detected by a free space powermeter. The QWP and HWP are then adjusted to minimize the detected power, with the final HWP angle designated as the V state for the idler arm. The output power difference between HWP's H and V position is 37 dB which is limited by the extinction ratio of the polarization components. A similar procedure is

employed for the signal arm, using a laser at 1539.37 nm. Once the waveplates' angles are calibrated, it is crucial that the QWPs remain stationary during the two-photon interference measurement to ensure accuracy. In the local measurement case, once the photon pairs are collected with the UHNA7 fiber, the insertion loss from Sagnac loop to the fiber connector before SNSPD is 2.74 dB for signal arm and 2.72 dB for idler arm. This includes all the fiber based and free space optical components in the experiment.

#### 4.5 Single photon detection and coincidence counting

In the 93 km entanglement distribution experiment, the single photons are detected with SNSPDs, with the efficiency for idler channel at 45% while efficiency for signal channel is at 78%. Single photon count rate is 4.8 kcps for signal arm and 5.6 Mcps for idler arm. The delay cause by the deployed fiber is 457,369,970 ps which is equal to the distance measured by OTDR. The coincidence window  $\tau_{cw}$  used in local measurement is 200 ps while  $\tau_{cw}$  with deployed fiber is 60 ps for accidental suppression and higher CAR. The narrow  $\tau_{cw}$  does result in a lower photon pair rate. Reducing the background noise (detector dark counts, Raman noise in the source, and stray light coupling into the fiber network) should further improve the CAR and fidelity. When the deployed fiber distance is extended to 155 km, the singles count rate on signal and idler arm are around 15 kcps and 40 kcps respectively. Although this low single count rate will not saturate the detector, the SNSPD are set to 56% efficiency to reduce the dark count to 10 cps. The optical delay caused by the 62 km fiber is 302,113,173 ps which is equal to the length characterization by OTDR.

#### 4.6 Fiber link information

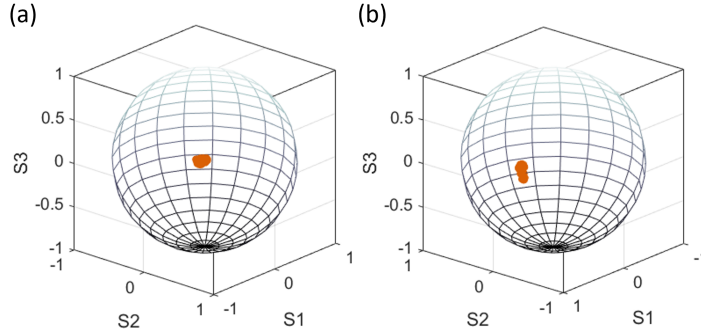


**Fig. 7 Polarization long term stability measurement.** Polarized light at 1539.37 nm or 1561.01 nm is sent into the 93 km NUS-SUTD-NUS fiber link (a) and the 62 km NUS-NTU-NUS fiber link (b). The output polarization is continuously recorded for 8 hours to monitor long-term polarization drift of respective deployed fibers.

A measurement of polarization stability of deployed fibers over a continuous period of 8 hours is conducted and the polarization state rotates  $10.75^\circ$  (93 km link) and  $12.63^\circ$  (62 km link) on the Poincare sphere. The results in Fig. 7. (a, b) indicate a relatively stable polarization behavior.

Additionally, signal crosstalk from other channels in metropolitan fiber networks can introduce background noise, which also affects the quantum state fidelity. The NUS-SUTD-NUS (or NUS-NTU-NUS) fiber loop experiences approximately 4 Mcps (2 kcps) of background noise without spectral filtering. This noise is broadband and can be effectively mitigated using a 0.8 nm bandwidth DWDM filter. After inserting the filter, the background noise in both channels is reduced to less than 200 cps.

## Acknowledgements

This research is supported by the National Research Foundation, Singapore, and A\*STAR under its CQT Bridging Grant and Quantum Engineering Programme (Award No. NRF2021-QEP2-01-P02), QEP2 grant: NRF2021-QEP2-01-P01, and US Air Force grant (FA2386-21-1-0076). D. Tan acknowledges funding from the National Research Foundation, Singapore, and A\*STAR under its QEP 2.0 Programme (Award No. NRF2022-QEP2-01-P08), the National Research Foundation Investigatorship (NRF-NRFI08-2022-0003) and the Ministry of Education Tier 2 Grant (Award No. MOE2019-T2-2-178). We acknowledge funding support from the National Research Foundation, Singapore and A\*STAR under its Quantum Engineering Programme (National Quantum-Safe Network, NRF2021-QEP2-04-P01) and Netlink Trust for the provisioning of the fiber network. The authors acknowledge the assistance of setup alignment and literature review from Arya Chowdhury, and Lim En Teng, and consultation from Dr. Tanvirul Islam.

## Declarations

The authors declare no conflicts of interest.

## References

- [1] Liao, S.-K., Cai, W.-Q., Liu, W.-Y., Zhang, L., Li, Y., Ren, J.-G., Yin, J., Shen, Q., Cao, Y., Li, Z.-P., *et al.*: Satellite-to-ground quantum key distribution. *Nature* **549**(7670), 43–47 (2017)
- [2] Yin, J., Cao, Y., Li, Y.-H., Ren, J.-G., Liao, S.-K., Zhang, L., Cai, W.-Q., Liu, W.-Y., Li, B., Dai, H., *et al.*: Satellite-to-ground entanglement-based quantum key distribution. *Physical review letters* **119**(20), 200501 (2017)
- [3] Villar, A., Lohrmann, A., Bai, X., Vergoossen, T., Bedington, R., Perumangatt, C., Lim, H.Y., Islam, T., Reezwana, A., Tang, Z., *et al.*: Entanglement demonstration on board a nano-satellite. *Optica* **7**(7), 734–737 (2020)

- [4] Yin, J., Li, Y.-H., Liao, S.-K., Yang, M., Cao, Y., Zhang, L., Ren, J.-G., Cai, W.-Q., Liu, W.-Y., Li, S.-L., *et al.*: Entanglement-based secure quantum cryptography over 1,120 kilometres. *Nature* **582**(7813), 501–505 (2020)
- [5] Ursin, R., Tiefenbacher, F., Schmitt-Manderbach, T., Weier, H., Scheidl, T., Lindenthal, M., Blauensteiner, B., Jennewein, T., Perdigues, J., Trojek, P., *et al.*: Entanglement-based quantum communication over 144 km. *Nature physics* **3**(7), 481–486 (2007)
- [6] Yin, J., Ren, J.-G., Lu, H., Cao, Y., Yong, H.-L., Wu, Y.-P., Liu, C., Liao, S.-K., Zhou, F., Jiang, Y., *et al.*: Quantum teleportation and entanglement distribution over 100-kilometre free-space channels. *Nature* **488**(7410), 185–188 (2012)
- [7] Wengerowsky, S., Joshi, S.K., Steinlechner, F., Zichi, J.R., Dobrovolskiy, S.M., Molen, R., Los, J.W., Zwiller, V., Versteegh, M.A., Mura, A., *et al.*: Entanglement distribution over a 96-km-long submarine optical fiber. *Proceedings of the National Academy of Sciences* **116**(14), 6684–6688 (2019)
- [8] Wengerowsky, S., Joshi, S.K., Steinlechner, F., Zichi, J.R., Liu, B., Scheidl, T., Dobrovolskiy, S.M., Molen, R.v.d., Los, J.W., Zwiller, V., *et al.*: Passively stable distribution of polarisation entanglement over 192 km of deployed optical fibre. *npj Quantum Information* **6**(1), 5 (2020)
- [9] Neumann, S.P., Buchner, A., Bulla, L., Bohmann, M., Ursin, R.: Continuous entanglement distribution over a transnational 248 km fiber link. *Nature Communications* **13**(1), 6134 (2022)
- [10] Rahmouni, A., Kuo, P., Li-Baboud, Y.-S., Burenkov, I., Shi, Y., Jabir, M., Lal, N., Reddy, D., Merzouki, M., Ma, L., *et al.*: Metropolitan-scale entanglement distribution with co existing quantum and classical signals in a single fiber. *arXiv preprint arXiv:2402.00617* (2024)
- [11] Appas, F., Baboux, F., Amanti, M.I., Lemaître, A., Boitier, F., Diamanti, E., Ducci, S.: Flexible entanglement-distribution network with an algaas chip for secure communications. *npj Quantum Information* **7**(1), 118 (2021)
- [12] Suo, J., Dong, S., Zhang, W., Huang, Y., Peng, J.: Generation of hyper-entanglement on polarization and energy-time based on a silicon micro-ring cavity. *Optics express* **23**(4), 3985–3995 (2015)
- [13] Takesue, H., Fukuda, H., Tsuchizawa, T., Watanabe, T., Yamada, K., Tokura, Y., Itabashi, S.-i.: Generation of polarization entangled photon pairs using silicon wire waveguide. *Optics express* **16**(8), 5721–5727 (2008)
- [14] Li, Y.-H., Zhou, Z.-Y., Feng, L.-T., Fang, W.-T., Liu, S.-l., Liu, S.-K., Wang, K., Ren, X.-F., Ding, D.-S., Xu, L.-X., *et al.*: On-chip multiplexed multiple entanglement sources in a single silicon nanowire. *Physical Review Applied* **7**(6), 064005

(2017)

- [15] Sharma, S., Venkataraman, V., Ghosh, J.: Silicon photonic wires for broadband polarization entanglement at telecommunication wavelengths. *Physical Review Applied* **18**(4), 044043 (2022)
- [16] Du, J., Chen, G.F., Gao, H., Grieve, J.A., Tan, D.T., Ling, A.: Demonstration of a low loss, highly stable and re-useable edge coupler for high heralding efficiency and low  $g^{(2)}(0)$  soi correlated photon pair sources. *Optics Express* **32**(7), 11406–11418 (2024)
- [17] Wen, W., Yan, W., Lu, C., Lu, L., Wu, X., Lu, Y., Zhu, S., Ma, X.-S.: Polarization-entangled quantum frequency comb from a silicon nitride microring resonator. *Physical Review Applied* **20**(6), 064032 (2023)
- [18] Zhang, M., Feng, L.-T., Zhou, Z.-Y., Chen, Y., Wu, H., Li, M., Gao, S.-M., Guo, G.-P., Guo, G.-C., Dai, D.-X., *et al.*: Generation of multiphoton quantum states on silicon. *Light: Science & Applications* **8**(1), 41 (2019)
- [19] Chua, R., Grieve, J.A., Ling, A.: Fine-grained all-fiber nonlocal dispersion compensation in the telecommunications o-band. *Optics Express* **30**(9), 15607–15615 (2022)
- [20] Neumann, S.P., Ribezzo, D., Bohmann, M., Ursin, R.: Experimentally optimizing qkd rates via nonlocal dispersion compensation. *Quantum Science and Technology* **6**(2), 025017 (2021)
- [21] Boyd, R.W., Gaeta, A.L., Giese, E.: Nonlinear optics. In: *Springer Handbook of Atomic, Molecular, and Optical Physics*, pp. 1097–1110. Springer, ??? (2008)
- [22] Miloshevsky, A., Cohen, L.M., Myilswamy, K.V., Alshowkan, M., Fatema, S., Lu, H.-H., Weiner, A.M., Lukens, J.M.: Cmos photonic integrated source of broadband polarization-entangled photons. *Optica Quantum* **2**(4), 254–259 (2024)
- [23] Zhuang, S.-C., Li, B., Zheng, M.-Y., Zeng, Y.-X., Wu, H.-N., Li, G.-B., Yao, Q., Xie, X.-P., Li, Y.-H., Qin, H., *et al.*: Ultrabright-entanglement-based quantum key distribution over a 404-km-long optical. *arXiv preprint arXiv:2408.04361* (2024)
- [24] Gisin, N., Ribordy, G., Tittel, W., Zbinden, H.: Quantum cryptography. *Reviews of modern physics* **74**(1), 145 (2002)
- [25] Shi, Y., Moe Thar, S., Poh, H.S., Grieve, J.A., Kurtsiefer, C., Ling, A.: Stable polarization entanglement based quantum key distribution over a deployed metropolitan fiber. *Applied Physics Letters* **117**(12) (2020)
- [26] Zhang, X., Zhang, H., Chua, R.M., Eng, J., Meunier, M., Grieve, J.A., Gao,

- W., Ling, A.: Polarization-encoded quantum key distribution with a room-temperature telecom single-photon emitter (2024). <https://arxiv.org/abs/2409.17060>
- [27] Antonelli, C., Shtaif, M., Brodsky, M.: Sudden death of entanglement induced by polarization mode dispersion. *Physical review letters* **106**(8), 080404 (2011)
- [28] Lu, C.-Y., Cao, Y., Peng, C.-Z., Pan, J.-W.: Micius quantum experiments in space. *Reviews of Modern Physics* **94**(3), 035001 (2022)
- [29] Ong, J.R., Kumar, R., Mookherjea, S.: Ultra-high-contrast and tunable-bandwidth filter using cascaded high-order silicon microring filters. *IEEE Photonics Technology Letters* **25**(16), 1543–1546 (2013)
- [30] Luo, L.-W., Ophir, N., Chen, C.P., Gabrielli, L.H., Poitras, C.B., Bergmen, K., Lipson, M.: Wdm-compatible mode-division multiplexing on a silicon chip. *Nature communications* **5**(1), 1–7 (2014)
- [31] Kumar, R.R., Wu, X., Tsang, H.K.: Compact high-extinction tunable crow filters for integrated quantum photonic circuits. *Optics Letters* **45**(6), 1289–1292 (2020)
- [32] Cui, L., Wang, J., Li, J., Ma, M., Ou, Z., Li, X.: Programmable photon pair source. *APL Photonics* **7**(1) (2022)
- [33] Ong, K.Y.K., Chen, G.F., Xing, P., Gao, H., Tan, D.T.: Dispersion compensation of high-speed data using an integrated silicon nitride ring resonator. *Optics Express* **30**(9), 13959–13967 (2022)
- [34] Joshi, C., Farsi, A., Clemmen, S., Ramelow, S., Gaeta, A.L.: Frequency multiplexing for quasi-deterministic heralded single-photon sources. *Nature communications* **9**(1), 847 (2018)
- [35] Zheng, Y., Zhai, C., Liu, D., Mao, J., Chen, X., Dai, T., Huang, J., Bao, J., Fu, Z., Tong, Y., *et al.*: Multichip multidimensional quantum networks with entanglement retrievability. *Science* **381**(6654), 221–226 (2023)
- [36] Xie, Z., Zhong, T., Shrestha, S., Xu, X., Liang, J., Gong, Y.-X., Bienfang, J.C., Restelli, A., Shapiro, J.H., Wong, F.N., *et al.*: Harnessing high-dimensional hyperentanglement through a biphoton frequency comb. *Nature Photonics* **9**(8), 536–542 (2015)
- [37] Chapman, J.C., Graham, T.M., Zeitler, C.K., Bernstein, H.J., Kwiat, P.G.: Time-bin and polarization superdense teleportation for space applications. *Physical Review Applied* **14**(1), 014044 (2020)
- [38] Ma, C., Sacher, W.D., Tang, Z., Mikkelsen, J.C., Yang, Y., Xu, F., Thiessen, T., Lo, H.-K., Poon, J.K.: Silicon photonic transmitter for polarization-encoded

quantum key distribution. *Optica* **3**(11), 1274–1278 (2016)

- [39] Zhang, Q., Wu, K., Poon, A.W.: Polarization entanglement generation in silicon nitride waveguide-coupled dual microring resonators. *Optics Express* **32**(13), 22804–22816 (2024)